sLLE: Spherical Locally Linear Embedding with Applications to Tomography

Yi Fang
Purdue University
Purdue University, West Lafayette, IN 47907
fang4@purdue.edu

S.V. N. Vishwanathan
Purdue University
Purdue University, West Lafayette, IN 47907
vishy@stat.purdue.edu

Mengtian Sun
Purdue University
Purdue University, West Lafayette, IN 47907
sun84@purdue.edu

Karthik Ramani
Purdue University
Purdue University, West Lafayette, IN 47907
ramani@purdue.edu

Abstract

The tomographic reconstruction of a planar object from its projections taken at random unknown view angles is a problem that occurs often in medical imaging. Therefore, there is a need to robustly estimate the view angles given random observations of the projections. The widely used locally linear embedding (LLE) technique provides nonlinear embedding of points on a flat manifold. In our case, the projections belong to a sphere. Therefore, we extend LLE and develop a spherical locally linear embedding (sLLE) algorithm, which is capable of embedding data points on a non-flat spherically constrained manifold. Our algorithm, sLLE, transforms the problem of the angle estimation to a spherically constrained embedding problem. It considers each projection as a high dimensional vector with dimensionality equal to the number of sampling points on the projection. The projections are then embedded onto a sphere, which parametrizes the projections with respect to view angles in a globally consistent manner. The image is reconstructed from parametrized projections through the inverse Radon transform. A number of experiments demonstrate that sLLE is particularly effective for the tomography application we consider. We evaluate its performance in terms of the computational efficiency and noise tolerance, and show that sLLE can be used to shed light on the other constrained applications of LLE.

1. Introduction

Tomography is defined as the process of recovering an object from measurements that are line integrals of that object at some set of known view angles [7]. It has been successfully applied in various applications such as medical imaging, synthetic aperture radar (SAR), and Cryo-electron microscopy (cryoEM) for structuring viruses over the past decades [7, 17, 1, 9, 10, 5]. However, in some special situations it is not easy to obtain the view angles accurately. For example, a patient might move during a long scanning period, and this can result in uncertainty of view angles. Similarly, the data acquisition of single particle cryoEM are the line integrals of many identical copies of virus molecules at random orientations. One would still like to reconstruct the object in these cases. One way to solve this problem is to embed the observed measurements, P_θ, generated from a unknown view angle θ into a sphere (see Figure.1 (A) for illustration). In other words, given a number of the observations, the reconstruction problem boils down to the estimation of view angles for each projection.

The widely used locally linear embedding (LLE) technique provides nonlinear embedding of points on a flat manifold. In our case, the observations belong to a sphere. Therefore, we extend LLE and develop a spherical locally linear embedding (sLLE) algorithm, which is capable of embedding data points on a non-flat spherically constrained manifold. Both LLE and our extension sLLE can be viewed as dimensionality reduction techniques. Dimensionality reduction has become an important and challenging research topic in machine learning with applications in areas as diverse as image processing, computer vision, pattern recognition and biological image processing. The aim of dimensionality reduction is to mine the hidden (intrinsic) parameters for high-dimensional data. This principle inspires us to adapt dimensionality reduction technique to reduce the observed projection data to its intrinsic low dimensional representation: its corresponding view angle.

1.1. From LLE to sLLE

Recent years have seen an explosive growth of interest and activity on developing algorithms for nonlinear di-

mensionality reduction, for instance, isometric mapping (ISOMAP), locally linear embedding (LLE) and their variations [18, 14, 22, 19]. These algorithms first learn the intrinsic geometry of a neighborhood and non-linearly map the high dimensional data points into a lower dimensional manifold by preserving the learned geometric information.

LLE, in particular, has been successfully applied to a number of problems in areas as diverse as image processing, computer vision, and pattern recognition just to name a few. The non-iterative version of LLE starts by finding the neighbors for each data point, then reconstructs the weights for approximating the local geometry. It then attempts to find the coordinates in an embedded space where the local geometric structure is approximately preserved; this is done by solving an eigenvalue problem. Our sLLE (spherical LLE) algorithm is derived as an extension to LLE by incorporating the natural spherical constraints that occur in our application. Specifically, our modification will focus on the last step of finding the embedded coordinates in the low-dimensional space. With this modification, sLLE is able to solve the problem of the estimation of the view angles for tomographic reconstruction [2, 3, 13, 6]. As we show in this paper, this simple constraint allows us to accurately solve the tomographic reconstruction problem even when the view angles are not known.

Based on sLLE, we propose a generalized tomographic reconstruction procedure which does not require knowledge of acquisition of the view angles. As shown in Figure 1, the generalized framework consists of three steps. The measurements are obtained from a random set of view angles, they are then sorted by using the sLLE based reorganization algorithm, and the reconstruction of the image from the ordered projections is completed by using the inverse Radon transform.

The main contribution of the proposed method is twofold: 1) A modification of LLE to take into account spherically constrained embedded points, and 2) the development of a sLLE based scheme for application of view angle estimation. This paper is organized as follows. We describe the derivation of sLLE and the computational scheme for the estimation of view angles in Section 2. Experiments are reported in Section 3. The paper concludes with a Discussion.

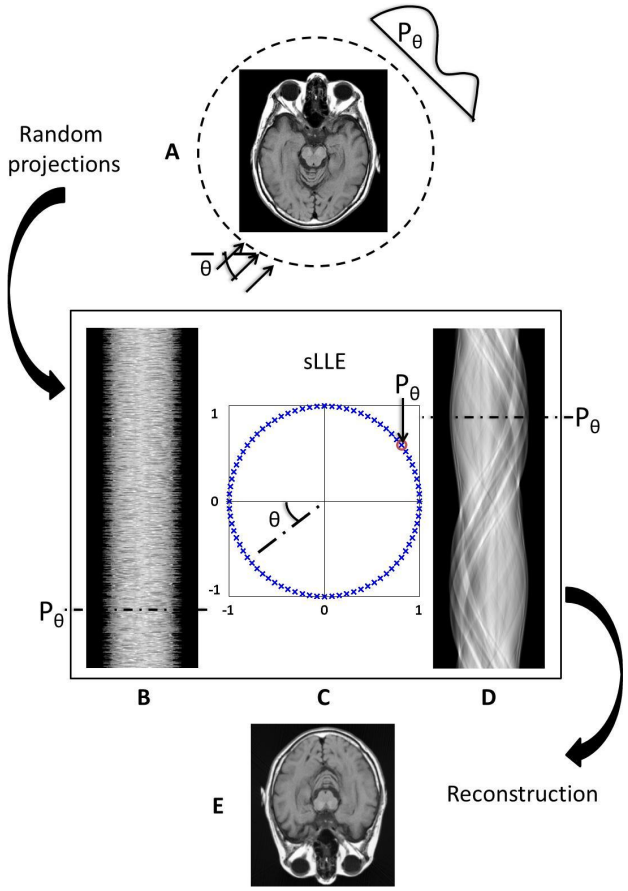

Figure 1. sLLE reconstruction flowchart. Figure (A) illustrates a measurement that is observed at a view angle θ. A number of such measurements are obtained at various angles θ and are stacked together in Figure (B). Each row denotes a measurement and we highlight one such measurement P_θ in the figure. As seen in Figure (C) our sLLE algorithm is used to embed the measurements on a circle with each point on the circle associated with one projection (see P_θ marked on the circle). The embedding of projections on the circle essentially sort the projections according to their relative view angles. Figure (D) shows the sorted projection data according to their relative view angles provided by embedding in Figure (C). Figure (E) displays the reconstructed image from the sorted projection data by using the inverse Radon transform. The reconstructed image is subject to a global rotation transform of the original image.

2. Methods

2.1. Tomographic Reconstruction

In the setting we consider, various measurements P_θ are obtained at view angles θ (Figure 1 (A)). One can view these measurements as projections that are line integrals of the image along the viewing direction θ. A set of such projections are stacked together into a high dimensional vector (PVector) $\overrightarrow{P_\theta} = (P(t_1), P(t_2), \ldots, P(t_n))$ where $t_1, t_2, \ldots, t_n$ are equally spaced sampling points and n is the dimensionality of the vector (see Figure 1 (B)). The Fourier transform of the PVector can also be viewed as a high dimensional vector (FTVector), and is represented as $\overrightarrow{F} = (F(\rho_1), F(\rho_2), \ldots, F(\rho_n))$ where $\rho_1, \rho_2, \ldots, \rho_n$ are equally spaced sampling points on the Fourier transform, and as before, n is the dimensionality of the vector. According to the Fourier slice theorem [12], each projection has a unique Fourier transform. Therefore sorting projections in a

space domain is equivalent to orienting their corresponding Fourier transforms in a frequency domain. As the view angles are expected to be embedded on a circle, a FTVector (a slice), $\overrightarrow{F}$ is intrinsically restricted to lie on a circle Mathematically, the FTVector $\overrightarrow{F_i} = (F_i(\rho_1), F_i(\rho_2), \ldots, F_i(\rho_n))$ could be intrinsically reduced to a two dimensional point $\overrightarrow{X_i} = (X_i(1), X_i(2))$ on a circle, where i denotes the i-th projection and 1 and 2 denote the principal axes of Cartesian coordinate respectively. The FTVectors can be oriented based on the corresponding two dimensional point set $\{\overrightarrow{X_i}, i \in (1, 2, \ldots, n)\}$ where n is the number of points. This dimensionality reduction of the projection data is illustrated in Figure 1 (A) to Figure 1 (C). The red point on the circle corresponds a specific PVector (P_θ) in Figure 1 (A). All of the PVectors are then sorted according to the estimated view angles in Figure 1 (C) and the Figure 1 (D) shows the sorted projections. This figure is sometimes called a sinogram in tomography.

Note that, there are two reasons to transform the PVector to the Fourier domain before applying dimensionality reduction. First, it is easier to reduce the influence of noise by band limiting the frequency. If the image is very noisy, then the signal in the low frequency range has signal-to-noise ratios close to one while the signal in the high frequency range has signal-to-noise ratios close to zero. Second, the magnitude of the Fourier vector is invariant to the center shift of the image. Thus, even when the image shifts during projection, the distance would not be affected if the computation is only based on the magnitude of the Fourier values.

2.2. Deriving sLLE from LLE

We now describe the sLLE algorithm which is used to embed the FTVector from the above section into a sphere. There are basically three steps involved. In the first step, we find the K nearest neighbors (KNN) for each point [4]. We reconstruct the optimal local weights for each point from its nearest neighbors in the second step, and the third step we perform the embedding by preserving the reconstruction weights of all of the points on a sphere. The first two steps are identical to the original LLE algorithm and we refer the reader to [14] for more details.

2.2.1 KNN and Weight Reconstruction

Suppose X is a set of $N \times P$ points where N denotes the number of the points and P is the dimensionality of the one data point. Let x_i denote the i-th point. The KNN algorithm first computes the nearest neighbors for each data point. Then, with the assumption that neighbors lie on a small linear region of a non-linear manifold, each point x_i is approximated by a weighted linear combination of its K nearest neighbors. To reconstruct weight matrix W, the following least square optimization is solved:

$$\min_W \left\{ \sum_{i=1}^{N} \|x_i - \sum_{j=1}^{K} W_{(i,j)} x_j\| \right\}, \tag{1}$$

where $W_{(i,j)}$ denotes the weight between points x_i and its neighbor x_j.

2.2.2 Spherical Embedding

Let W be a $N \times N$ reconstructed weight matrix, and let $D \ll N$. Furthermore, define

$$Y = \begin{bmatrix} y_1 \\ y_2 \\ \vdots \\ y_n \end{bmatrix} \tag{2}$$

be a $N \times D$ matrix whose rows are the low dimensional embedding vectors y_i that we are interested in computing. Given the matrix W, computing Y can be posed as the following optimization problem:

$$\begin{aligned} \phi(Y) &= \sum_i \left| y_i - \sum_j W_{(i,j)} y_j \right|^2 \\ &= \operatorname{tr}\left((Y - WY)(Y - WY)^\top \right). \end{aligned} \tag{3}$$

Using the identity $\operatorname{tr}(ABC) = \operatorname{tr}(CAB)$ we can rewrite the above objective function as

$$\begin{aligned} \phi(Y) &= \operatorname{tr}\left((Y - WY)^\top (Y - WY) \right) \\ &= \operatorname{tr}\left(Y^\top Y - Y^\top W^\top Y - Y^\top W Y - Y^\top W^\top W Y \right) \\ &= \operatorname{tr}\left(Y^\top (I - W^\top - W - W^\top W) Y \right) \\ &= \operatorname{tr}\left(Y^\top \underbrace{(I - W)^\top (I - W)}_{:=M} Y \right) \\ &= \operatorname{tr}\left(Y^\top M Y \right) \end{aligned} \tag{4}$$

Minimizing the above objective function yields the LLE embedding of X. However, in our case we want the embedded points to lie on an unit sphere. To enforce this constraint we introduce a diagonal matrix B and define $Z := \sqrt{B} Y$. We will require that rows of Z are normalized, that is, $z_i^\top z_i = 1$ for $i = 1, \ldots, N$. This yields the following difficulty to optimize objective function:

$$\min_{Y,B} \operatorname{tr}\left(Y^\top M Y \right) \text{ s.t. } Y^\top B Y = Z^\top Z = I. \tag{5}$$

We propose an iterative scheme to solve the above problem.

- Y **Step:** Compute Y by solving

$$\min_{Y} \operatorname{tr}\left(Y^\top M Y\right) \text{ s.t. } Y^\top B Y = Z^\top Z = I. \quad (6)$$

Appealing to Theorem 1.2 in [15] shows that the solution is given by the first D eigenvalues of the generalized eigenvalue problem $MY = \gamma BY$.

- B **Step:** We want B such that the diagonal elements of $\sqrt{B}YY^\top\sqrt{B}$ are all ones. This can be satisfied by setting $B = \operatorname{diag}\left(\frac{1}{y_i^\top y_i}\right)$.

Our iterative scheme starts with $B = I$ and iterates until both Y and B do not change. It outputs $Z = \sqrt{B}Y$ as the solution for the spherical embedding with unit norm.

2.2.3 Computational Scheme

Reconstructing the weight matrix Given the Fourier transform vectors for all of the projections, we first build the K nearest neighbors for each FTvector based on the L_2 distance defined in (7). Note that a number of standard ways of measuring the distance between two high dimensional vectors have been proposed. Examples include the L_1 norm, L_2 norm, λ^2 measure, and Bhattacharyya distance. In this work, we adopt the widely used L_2 norm.

$$d_{L_2}(A, B) = \|\overrightarrow{F_A} - \overrightarrow{F_B}\| \quad (7)$$

where $\overrightarrow{F_A}$ and $\overrightarrow{F_B}$ denote differently oriented FTVectors respectively.

To reconstruct the weight matrix W, we will solve the following least square optimization to minimize the reconstruction error:

$$\varepsilon(W) = \sum_{i=1}^{n} \|x_i - \sum_j W_{(i,j)} x_j\| \quad (8a)$$

$$\text{s. t. } \sum_j W_{(i,j)} = 1 \quad (8b)$$

where x_i denotes the i-th FTvector and j denotes its j-th neighbor and W is the reconstruction weight matrix

Determining view angles Given the weight matrix W, the view angles are determined as follows:

1. Apply sLLE for spherical embedding of FTVectors with reduced dimensionality $D = 2$. This yields the two dimensional representation for each projection.

2. Let $\overrightarrow{Z_i}$ denote the i-th embedded point. Apply the inverse trigonometric function, arctangent, to the coordinates of embedded points for calculating the initial set of view angles,

$$\varphi_i = \arctan\left(\frac{Z_i(2)}{Z_i(1)}\right). \quad (9)$$

3. Sort the view angles $(\varphi_1, \varphi_2, \ldots, \varphi_n)$, uniformly rearrange them along the circle, and associate the refined view angle set to the original projections set.

3. Experimental Results

sLLE was implemented on a Pentium D 3.2GHz computer with 2G RAM running Windows XP. Our focus is on 2 dimensional tomographic reconstruction with unknown view angles.

3.1. Orienting Points on a Circle

In this experiment, we test sLLE using a toy model. This test starts by generating a uniform set of data points on a circle with equal angular sampling. The number of the data points, N, is set at 100. The data is then randomly shuffled and we use the sLLE to re-organize the points and embedded them on a circle. In this experiment, each data point is two dimensional. Figure 2 (A) illustrates the original data points on the circle (blue cross). We find the K (we use 15 here) nearest neighbors for each data point according to the L_2 distance metric. The weight matrix is reconstructed based on (8a). In Figure 2 (B), we plot the estimated coordinates as red circles and super-impose the original data which is plotted as blue crosses. Note that the estimated data points are only slightly different from the original ones, which indicates the good performance of sLLE on the spherical constrained problems. Figure 2 (C) plots the results after further refinement of the initial estimated coordinates (see step 2 and 3 in section 2.2.3). It is clearly seen that refined coordinates (red circles) exactly match the original coordinates (blue crosses). To evaluate the estimation of the angle before the refinement, we calculate the mean squared error (MSE) for the estimated angles using original angles as ground truth. The MSE is 0.0036 between the original 100 points and the estimated ones, which is less than 6% of the angular sampling rate. This toy experiment mainly demonstrates the feasibility of our sLLE computational scheme for the spherically constrained problems. The applications of the sLLE on the more challenging tomographic reconstruction tasks will be discussed next.

3.2. Tomographic Reconstructions

In this experiment, we verify the performance of sLLE for view angles estimation with tomographic reconstructions of different types of images including a phantom image, one MR brain image, and two cryoEM density images. The MR images are chosen from the Whole Brain Atlas (http://www.med.harvard.edu/AANLIB/), which provides a large set of MR images for both normal and diseased brains. The cryoEM density images are available from the EM database (http://www.pdbj.org/emnavi/). In particu-

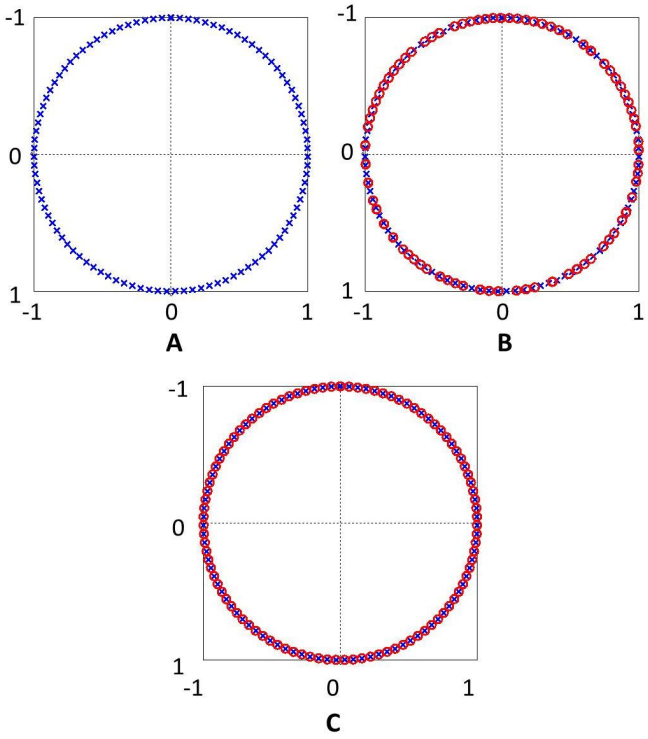

Figure 2. Toy experiment. Three figures show the reconstruction result from a toy experiment of orienting the points sampled from a circle. Figure (A) plots the sampled points on the circle (blue crosses). There are 100 points uniformly sampled on the circle. Figure (B) plots the estimated coordinates for the sampled points in (A). The estimated points are marked as red circles and the original sampled points are blue crosses. Figure (C) plots the results after further refinement. We find that the refinement leads to a exact overlap between the reconstructed points and original sampling points, which demonstrates the good performance of sLLE on this toy problem.

lar, we use the images with IDs 5030 and 1713 respectively in our experiments.

The comparison between LLE and sLLE is in terms of the quality of reconstruction. We used the procedure described in Section 2 for our experiments. For each image, we generate different number of the projections from a set of view angles ranging from 0° to 360°. The view angles are estimated based on the projections data using our proposed method, and the images are reconstructed by using an inverse Radon transform. We demonstrate the performance by comparison between the original and reconstructed images.

Figure 3 compares the original images (A_1, B_1, C_1, D_1) and the corresponding reconstructed images underneath. Figure 3 (A_2, B_2, C_2, D_2) illustrates the reconstruction results of original images by LLE, and Figure 3 (A_3, B_3, C_3, D_3) illustrates the reconstruction result of original images

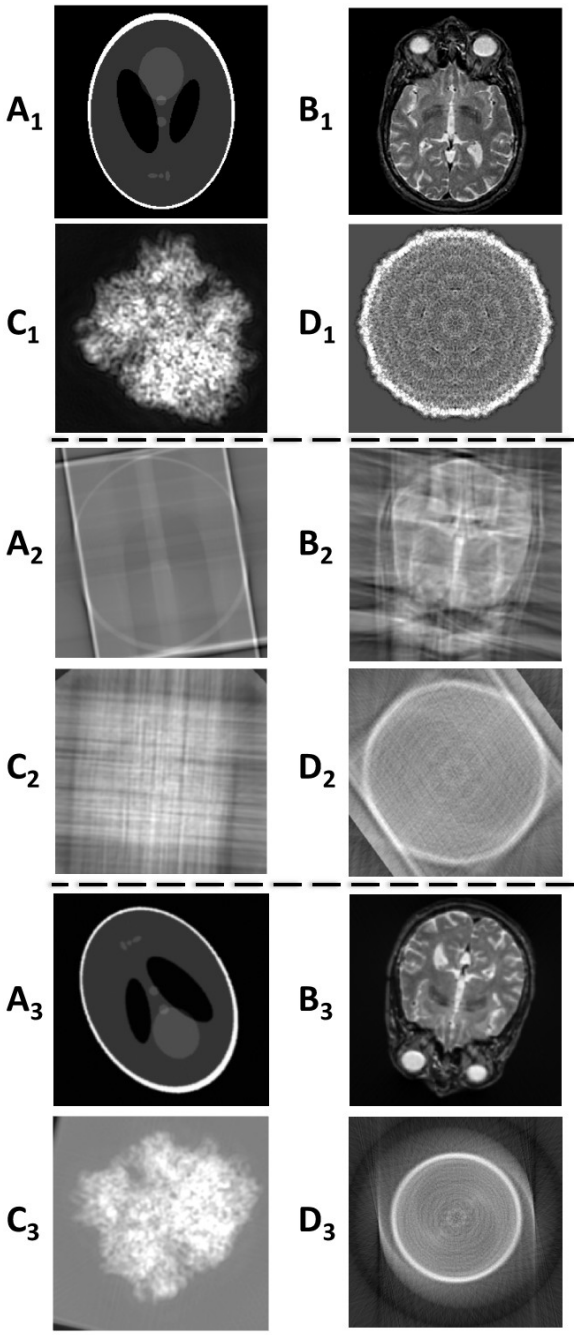

Figure 3. Comparison LLE and sLLE for tomographical reconstruction. Different types of the images are used in the comparison. Figure (A_1, B_1, C_1, D_1) depict the original phantom image, a MR brain image, a ribosome cryoEM image, and a Cyanophage cryoEM image, respectively. See the text for details. Figure (A_2, B_2, C_2, D_2) show the images as reconstructed by the LLE algorithm. Figure (A_3, B_3, C_3, D_3) are the images as reconstructed by sLLE. Visually one can observe that sLLE outperforms LLE in the reconstruction of non-symmetric images; the first three reconstructions reasonably recover the original images. However, sLLE fails in the last case because of the internally icosahedral symmetry of the virus structure.

$Image$	$PSNR$	MSE
Phantom	18.5353	0.0109
MR Brain	35.4612	0.0003
CryoEM-1	37.1278	0.0002
CryoEM-2	—	—

Table 1. Evaluation of Reconstruction Quality

by sLLE. It is clear that sLLE outperforms the LLE in these reconstruction problems. From the reconstructed images, we can also see that the first three images (Figure 3 (A_3, B_3, C_3) are well reconstructed subjected to an arbitrary rotation of the original images. Therefore, we find that the image can be reconstructed with a high quality if the images are not symmetric. Figure 3 (D_3) shows an unsuccessful reconstruction. This is due to the inherent symmetry of the image, a limitation of our sLLE method which we discuss further in Section 4. Note that the refinement of estimated angles has been applied on this experiment (see step 2 and 3 in section 2.2.3).

We further quantitatively verify the reconstruction performance of sLLE by comparing the original image with the reconstructed image. In our test, we cannot directly subtract the original from the reconstructed image as there is an arbitrary rotation of the reconstructed image. However, the registration of the two images can remove the effect of the arbitrary global rotation. In this experiment, the registration between original and reconstructed images is trivial as the correspondence between the randomly shuffled projections and the re-organized projections can be easily tracked. The global rotation angle can be easily retrieved by finding the difference between any corresponding pairs. For example, we can track all of the projections of the original image, find all of the relative positions in the re-organized projections sequence, and then compute the average of the rotation angle. We provide two quantitative measures for the reconstruction performance: one is the peak signal-to-noise ratio (PSNR), and the other is mean squared error (MSE), which are calculated using (10) and (11) below. The image on the left is the original image, the middle image is reconstructed from 512 projections and the image on the right is registered by the method described above. Table 1 presents the results of the evaluation of the reconstruction quality. The result demonstrates that sLLE yields good quality reconstruction of a variety of images, which indicates that it is very useful in tomographic reconstruction with unknown view angles. The quantitative measures of MSE and PSNR are not available for CryoEM-2 image (last row in the table) because sLLE fails in the reconstruction in this test.

$$\text{MSE} := \frac{1}{mn}\sum_{i=0}^{m-1}\sum_{j=0}^{n-1}[I_1(i,j) - I_2(i,j)]^2 \qquad (10)$$

where I_1 and I_2 denote two images respectively, and m and n denotes the size of the image

$$\text{PSNR} = 20\log_{10}(\frac{MAX_I}{\sqrt{\text{MSE}}}) \qquad (11)$$

where MAX_I denotes the maximum possible pixel value in the input image.

3.3. Noise Robustness

In practice, the image is often corrupted by noise during the acquisition process. Therefore, it is of great interest to check if sLLE is robust to noise. We mainly focused on additive noise in our experiments. We chose the brain MR image as our experimental subject, generated a set of the projections from 512 view angles randomly, and added zero mean Gaussian noise to the recorded projections. The standard deviation of the additive noise is determined as follows:

$$\text{SNR} = 10\log_{10}(\frac{Signal}{Noise}) \qquad (12)$$

where Signal and Noise are the standard deviation of the noiseless projections and the noise respectively.

Figure 4 shows the reconstruction results. Our proposed method demonstrates good performance for the noisy projections. From the Figure 4 (D-F), we can conclude that the reconstruction quality is only slightly affected by the noise if the value of the SNR is above 5B. We can find that sLLE works even when SNR drops down to 0.5dB (see Figure 4 (A)), which is worse than that encountered in most real world scenarios.

4. Discussion and Conclusions

LLE has demonstrated its applicability in various areas including pattern recognition, computer vision, image processing, and medicine. While it is a versatile dimensionality reduction technique, LLE is not able to embed the points on a non-flat manifold such as a sphere. This limits the applicability of LLE in certain situations. In this paper, we propose a novel approach to constrain the embedding points on a sphere. The extension of LLE leads to a new dimensional reduction algorithm, the spherical locally linear embedding (sLLE). sLLE is shown to perform well on a set of phantom, MR and cryoEM images. We conclude by briefly summarizing the properties, application and limitations of our algorithm below.

Properties The proposed sLLE algorithm describes a new method for embedding high-dimensional data on a sphere with lower dimensionality. sLLE addresses both problems of dimensionality reduction and spherical constraint for the embedding. As a derivative of the LLE algorithm,

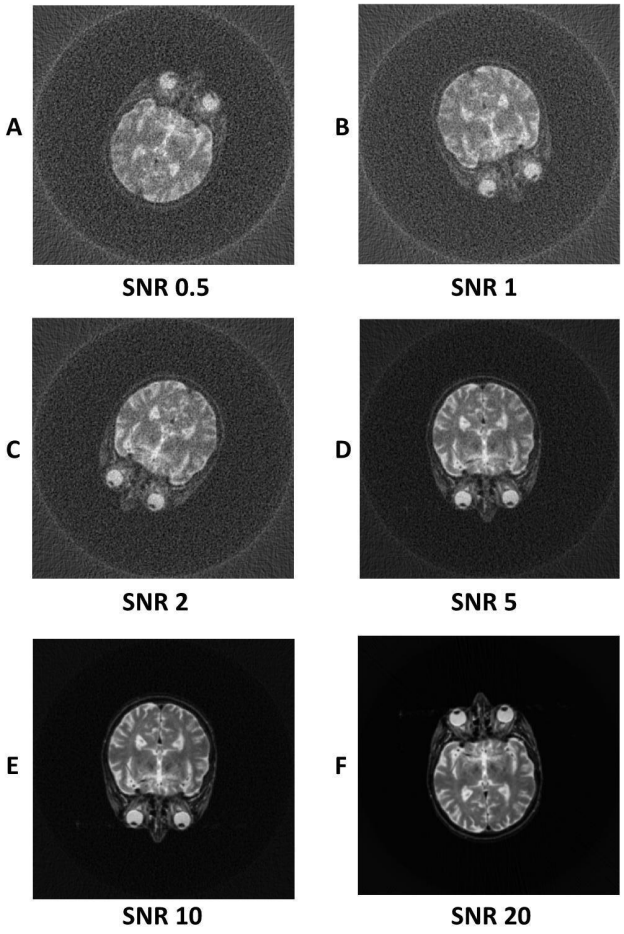

Figure 4. Robustness Test at Different Noise Levels. The six figures demonstrate the reconstruction results from noisy projections by sLLE. From Figure (A) to Figure (F), the projections are corrupted by the noise to increasingly different extents. The signal to noise ratio (SNR) underneath the figure indicates the level of the noise. We can conclude, based on the observation and comparison of the six reconstructed images, that our method is robust to noisy data. sLLE has shown a good performance in reconstruction when SNR is larger than 5 and performs reasonably even when the SNR is around 0.5 dB, in Figure (A).

sLLE inherits the attractive features of LLE such as nonlinear dimensionality reduction, unsupervised learning without much prior knowledge about the data, and global optimization. Primarily due to these advantages, LLE has gained an explosive popularity in a number of the research areas. Our sLLE expands the applicability of the LLE algorithm so that it can be used to map the high-dimensional data onto a sphere with lower dimensionality. In addition, sLLE leads to a general formulation of constrained dimensionality reduction. Our future work is on extending LLE to other natural constraints such as cylinder and tori.

Applications It is known that the estimation of view angles for projections is critical to improve reconstruction quality in the certain applications of tomography. We have applied the proposed framework for the tomography reconstruction in one of the cases. Extensions of the basic framework would further expand the applications of sLLE in different areas according to specific requirements. The sLLE framework would possibly be crucial to address the needs of patients in designing next generation tomographic equipments. For instance, nowadays, the patients are required to remain motionless during a long scanning period, which increases discomfort and anxiety of the patients and leads to measurement error and complications in analysis. Our method potentially can be used to minimize the effects of these constraints. In addition to medical images, we expect applications of sLLE where the global positioning of local data observations is crucial to perform inference on the data. Examples include sensor networks and NMR spectroscopy [16, 21]. The current embedding of the points in those application are currently not constrained by specific topology. However, the embedding of the data with constraints derived from prior knowledge would largely improve applicability of current techniques.

Limitations We note that sLLE suffers from some limitations. As we see in Figure 3, sLLE fails to provide a reasonable reconstruction for perfectly symmetric images. The symmetry results in identical projections from the different view angles. Therefore, it is not easy to associate these projections with different view angles as the projection data themselves are not distinguishable from each other. Instead, a possible solution would be to integrate the symmetry of the object before estimating the view angles. Symmetry estimation is an active research area in computer graphics, computer vision and image processing [8, 11, 20]. We will address this inherent limitation in our future work by incorporation potential symmetry information in our framework.

Acknowledgement

We would like to thank the Institute for Pure & Applied Mathematics (IPAM), a National Science Foundation (NSF) Math Institute at the University of California at Los Angeles (UCLA) for the fellowship to support Karthik Ramani. The experimental images are provided by the whole brain database from Harvard university. This work is partly based upon work supported by the National Science Foundation Partnership for Innovation Grant# 0917959 (3D Hub), NSF IIS Grant# 0535256, Donald W. Feddersen Chair Professorship support, Purdue University support for Faculty Study in a second discpline, and the School of Mechanical Engineering. Any opinions, findings, and conclusions or recommendations expressed in this material are those of the

author(s) and do not necessarily reflect the views of the National Science Foundation.

References

[1] S. Basu and Y. Bresler. Feasibility of tomography with unknown view angles. *IEEE Transactions on Image Processing*, 9:1107–1122, 2000. 1129

[2] S. Basu and Y. Bresler. Uniqueness of tomography with unknown view angles. *IEEE Transactions on Image Processing*, 9:1094–1106, 2000. 1130

[3] R. R. Coifman, Y. Shkolnisky, F. J. Sigworth, and A. Singer. Graph laplacian tomography from unknown random projections. *IEEE Transactions on Image Processing*, 17:1891–1899, 2008. 1130

[4] B. V. Dasarathy. Nearest neighbor (nn) norms: Nn pattern classification techniques. *Los Alamitos: IEEE Computer Society Press*, 1990. 1131

[5] Y. Fang, S. Murugappan, and K. Ramani. Estimating view parameters from random projections for tomography using spherical mds. *BMC Medical Imaging*, 10:12, 2010. 1129

[6] M. Georg, R. Souvenir, A. Hope, and R. Pless. Manifold learning for 4d ct reconstruction of the lung. *Computer Vision and Pattern Recognition Workshops,CVPRW '08*, pages 1–8, 2008. 1130

[7] H. Hiriyannaiah. X-ray computed tomography for medical imaging. *Signal Processing Magazine, IEEE*, 14(2):42–59, Mar 1997. 1129

[8] Y. Keller and Y. Shkolnisky. A signal processing approach to symmetry detection. *IEEE Transactions on Image Processing*, 15:2198–2207, 2006. 1135

[9] R. M. Lewitt and S. Matej. Overview of methods for image reconstruction from projections in emission computed tomography. *Proceedings of the IEEE*, 91(10):1588–1611, October 2003. 1129

[10] O. Llorca. Introduction to 3d reconstruction of macromolecules using single particle electron microscopy. *Acta Pharmacologica Sinica*, 26:1153–164, 2005. 1129

[11] N. J. Mitra, L. Guibas, and M. Pauly. Partial and approximate symmetry detection for 3d geometry. *ACM Transactions on Graphics*, 25(3):560–568, 2006. 1135

[12] L. Onural. Projection-slice theorem as a tool for mathematical representation of diffraction. *Signal Processing Letters, IEEE*, 14(1):43 –46, 2007. 1130

[13] M. Radermacher. Three dimensional reconstruction from random projections: Oriented alignment via radon transforms. *Ultramicroscopy*, 53:121–136, 1994. 1130

[14] S. Roweis and L. K. Saul. Nonlinear dimensionality reduction by locally linear embedding. *Science*, 290:2323–2326, December 2000. 1130, 1131

[15] A. H. Sameh and J. A. Wisniewski. A trace minimization algorithm for the generalized eigenvalue problem. *SIAM Journal on Numerical Analysis*, 19(6):1243–1259, 1982. 1132

[16] A. Singer. A remark on global positioning from local distances. *Proc. Natl. Acad. Sci. USA*, 105:9507–9511, 2007. 1135

[17] B. D. Smith. Cone-beam tomography: recent advances and a tutorial review. *Optical Engineering*, 29(5):524–534, 1990. 1129

[18] J. B. Tenenbaum, V. de Silva, and J. C. Langford. A global geometric framework for nonlinear dimensionality reduction. *Science*, 290:2319–2322, 2000. 1130

[19] S. Yan, D. Xu, B. Zhang, H.-J. Zhang, Q. Yang, and S. Lin. Graph embedding and extensions: A general framework for dimensionality reduction. *IEEE Transactions on Pattern Analysis and Machine Intelligence*, 29(1):40–51, 2007. 1130

[20] H. Zabrodsky, S. Peleg, and D. Avnir. Symmetry as a continuous feature. *IEEE Transactions on Pattern Analysis and Machine Intelligence*, 17:1154–1166, 1995. 1135

[21] L. Zhang, L. Liu, C. Gotsman, and S. J. Gortler. An as-rigid-as-possible approach to sensor network localization. *ACM Transactions on Sensor Networks*, 6(4):1–21, 2010. 1135

[22] Z. Zhang and J. Wang. MLLE: Modified locally linear embedding using multiple weights. In D. Koller, Y. Bengio, D. Schuurmans, L. Bottou, and A. Culotta, editors, *Advances in Neural Information Processing Systems 21*, pages 1593–1600, 2007. 1130